Journal of Materials Chemistry C

Accepted Manuscript

This article can be cited before page numbers have been issued, to do this please use: G. Bian, F. Zhao, T. Lau, C. Sheng, X. Lu, H. Du, C. Zhang, Z. Qu, H. Chen and J. Wan, *J. Mater. Chem. C*, 2019, DOI: 10.1039/C9TC02013F.

ROYAL SOCIETY OF CHEMISTRY

rsc.li/materials-c

Simply Planarizing Nonfused Perylene Diimide Based Acceptor Toward Promising Non-fullerene Solar Cells

View Article Online
DOI: 10.1039/C9TC02013F

Gao-Feng Bian[# a], Feng Zhao[# b], Tsz-Ki Lau[c], Chun-Qi Sheng[a], Xinhui Lu[c], Hui Du[a], Cheng Zhang[d], Zhi-Rong Qu*[a], Hongzheng Chen*[b] and Jun-Hua Wan*[a]

[#] Contributed equally

[a]. Key Laboratory of Organosilicon Chemistry and Material Technology of Ministry of Education, Hangzhou Normal University, Hangzhou, 310012, P. R. China.

*E-mail: wan_junhua@hznu.edu.cn, quzr@hznu.edu.cn

[b].State Key Laboratory of Silicon Materials, MOE Key Laboratory of Macromolecular Synthesis and Functionalization, & Department of Polymer Science and Engineering, Zhejiang University, Hangzhou 310027, P. R. China

*E-mail: hzchen@zju.edu.cn

[c]. Department of Physics, Chinese University of Hong Kong, New Territories, Hong Kong, P. R. China

[d]. State Key Laboratory Breeding Base of Green Chemistry Synthesis Technology, College of Chemical Engineering, Zhejiang University of Technology, Hangzhou 310014, P. R. China

KEYWORDS: organic solar cell, nonfullerene acceptor, perylene diimide, nonfused

Abstract

This work focuses on developing high-efficiency perylene diimide (PDI)-based small molecular nonfullerene acceptors with simply synthetic strategy. We reported a new electron acceptor, **Py-e-PDI**, obtained via cross-coupling four PDI units with planar pyrene core through ethynyl groups. Although the ring-fusion synthetic procedure was omitted, the large planar core as well as significantly reduced intramolecular steric hindrance endowed this nonfused PDI-tetramer derivative

with moderate planarity. Differing from most of PDI-tetramers with highly twisted geometries, **Py-e-PDI** could self-assemble into highly ordered structure. The inverted solar cells with PTB7-Th/**Py-e-PDI** blends exhibited the best power conversion efficiency up to 7.59%, which mainly resulted from the combined contribution of complementary absorption with a donor polymer, desirable aggregation and high electron mobility. Most importantly, this result demonstrates that simply planarizing 3D nonfused perylene diimide based acceptor is effective to improve the performance of the corresponding non-fullerene(NF) acceptors.

Introduction.

Conventional fullerene derivatives-based organic solar cells (OSCs) have achieved great successes in the past decade and their power conversion efficiencies (PCEs) had reached beyond 10% since 2014[1-4]. However, in recent several years, the further efforts of scientists to improve efficiency of this type OSCs had made no substantial progress due to the serious drawbacks of fullerene acceptors. Fullerene acceptors do not significantly contribute to light harvesting at wavelengths greater than 600 nm, and their energy levels cannot be fine-tuned to match the donor materials to maximize the open-circuit voltage (V_{oc}) and minimize the energy loss[5-6]. Recently, an emerging class of nonfullerene small molecule acceptors has rivaled the dominance of fullerene-based acceptors[7-9]. The single-junction non-fullerene OSCs can now achieve much higher PCEs (>14%) than fullerene-based ones[10-12]. And more, very recently, 17.3% PCE has been realized for a tandem device[13]. The great adjustability of molecular structures for small molecule acceptors offers a wide range of optoelectronic tunability.

Among the numerous non-fullerene electron acceptors, perylene diimide (PDI) based acceptors have been one of the most intensively studied and promising alternatives to fullerene derivatives because of their appropriate low-lying energy levels, high electron mobility and strong absorption in the visible region[14-17]. And it is worth mentioning that PDI, the most extensively used dyes in

industries, is readily scalable at low-cost, making it one of the few feasible candidates for commercial OSCs. Moreover, PDIs have complementary absorptions (300-600nm) with the typical narrow-band gap polymer donors, such as PTB7 and PTB7-Th. However, PDIs indicate the strong tendency of forming large aggregates due to their rigid polycyclic aromatic core. Therefore, a twisting strategy had been proposed to produce a twisted molecular geometry in PDI derivatives, which can suppress the strong aggregation and assure effective dissociation of photogenerated excitons into free charges[18]. However, a challenge involved in this effort is the difficulty to maintain the effective charge transport due to reduced π-π stacking between nonplanar PDIs. How much twisting would be needed? The development of PDI-based acceptors have experienced three stages, PDI monomers[19-20], twisted PDIs (dimmer[21-25], trimer[26-29] and tetramer[30-37]) and fused PDI [38-45]. Most of twisted PDIs showed PCE below 6%, while the fused PDIs obtained from oxidative cyclization exhibited significantly improved efficiency. It is obvious that in some PDI derivatives the twisted geometries greatly suppressed their crystallinities[29- 33]. After final oxidative cyclization, the highly twisted molecules could be changed to more planar molecules and crystallinity was thus significantly improved. According to the reported PDI based acceptors, a principle can be summarized as a guidance: when nanoscale phase separation is within a reasonable range, i.e., not too large for efficient exciton dissociation, the intermolecular π−π stacking is essential to enable the device with good charge transporting, which usually plays a dominant role in overall device performance. To develop high-efficiency PDI non-fullerene acceptor, the trade-off between the phase separation and strong π-π stacking should be considered.

Encouragingly, the efficiency of the champion PDI based device has been boosted to over 10%[39], which is very close to the high-efficiency NF acceptors with A-D-A structure, such as ITIC. However, to the best of our knowledge, most of PDI-based acceptors with PCE over 7% involved ring-fusion of PDI unit and only a few contained no fused structure[27-28, 46-49].

We focus on developing efficient PDI-based small molecular acceptors by simply synthetic procedure. A large molecular skeleton and slightly twisted configuration are considered as a suitable geometry to achieve high electron mobility and good film-forming property. Tetraphenylcarbon(TPC)[50], tetraphenylethylene (TPE)[30] and spirofluorene(SF)[32-33] cores possess three-dimension (3D) molecular structure, which usually results in highly twisted molecules. Moreover, one molecule with three or four PDI units in limited periphery would be overcrowded due to a big fused ring aromatic structure of PDI. Therefore, the periphery of core should be expanded. In 2017，Li and Wang et al reported a high-efficiency NF acceptor(**PBI-Por**), which has four PDI units connected at the meso-positions of a porphyrin ring through acetenyl groups[46]. In order to reduce intramolecular steric hindrance of PDI-based acceptors, C–C triple bonds were also inserted between 3D[51] or small[52] cores and PDI units as linkage to give PCEs of 5.84% and 6.0%, respectively (**Fig. 1**). And also, in the past two years, other types of small molecular acceptors with ethynyl group as linkers were developed[53-54]. Here, through a simply synthetic strategy, we constructed a planar four-PDI based electron acceptor(**Py-e-PDI**) by introducing planar pyrene unit as core, which is a four fused ring of polycyclic aromatic hydrocarbons (PAH). Similarly, C–C triple bond was used to link pyrene core and PDI units for the sake of enlarging the distance between pyrene core and PDI units (**Fig. 2**). A detailed investigation of the photophysical, electrochemical, and self-assembly properties was performed. This PDI derivative was also investigated as NF acceptors pairing PTB7-Th to fabricate OSCs.

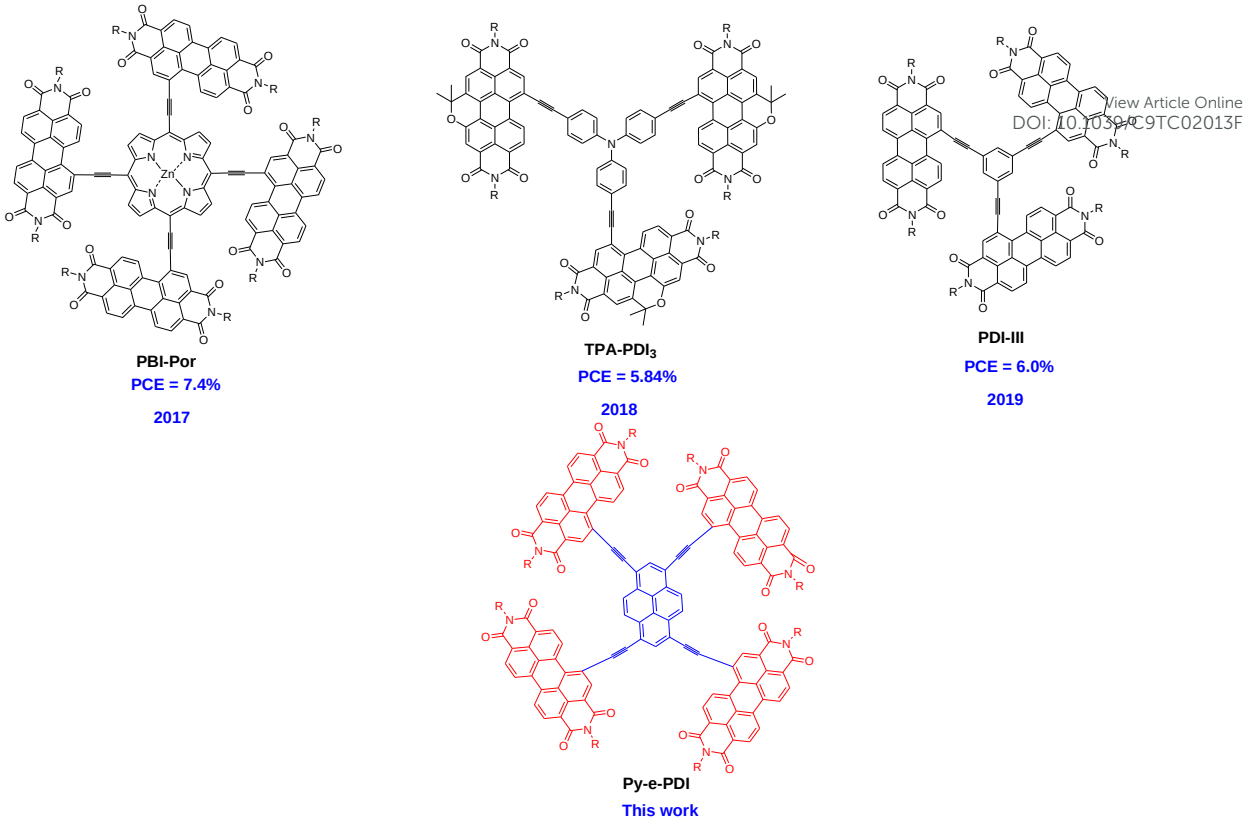

Fig. 1. The chemical structures of PDI-based acceptors with an acetylene spacer as linkage.

Result and Discussion

Synthesis and Characterization.

The synthesis of the **Py-e-PDI** involves only two steps reaction. Fig. **2a** shows the synthetic route to convert 1,3,6,8-tetrabromopyrene into corresponding tetra acetylene derivative (**3**) with high yield. Further Sonagashira coupling reaction between compound **3** and mono-brominated PDI (**Br-PDI**) at a molar ratio of 1:6 afforded the desired four-arm molecule **Py-e-PDI** in moderate yields (around 50%). Although the PDI units bear two branching alkyl chains, **Py-e-PDI** is less soluble in CH_2Cl_2 and $CHCl_3$ than in aromatics solvents, such as toluene, chlorobenzene, and dichlorobenzene. However, this limited solubility in CH_2Cl_2 does not affect purification procedure through sel-gel column chromatography using CH_2Cl_2 mixed with a small amount of hexane as eluent. The chemical structure of **Py-e-PDI** was confirmed by high-temperature ^1H NMR spectroscopy in *ortho*-dichlorobenzene-d_4 (**Fig. S2**), both low and high-resolution MALDI-TOF mass spectrometry, Raman spectra and elemental analysis.

(a)

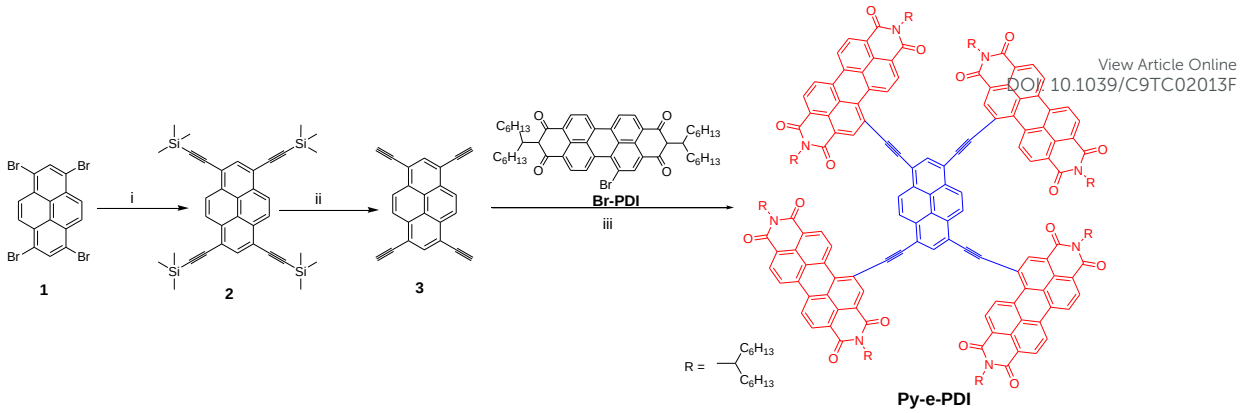

(b)

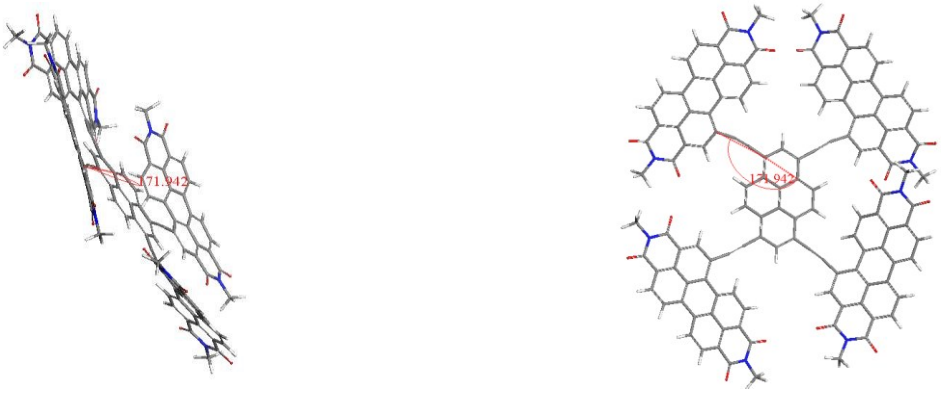

Fig. 2. (a) The chemical structure of **Py-e-PDI** and its synthetic route. (i) $Pd(PPh_3)_2Cl_2$, CuI, PPh_3, 6 equiv trimethysilylethyne, NEt_3/toluene, 80°C, 81%; (ii) K_2CO_3, MeOH; (iii) $Pd(PPh_3)_4$, CuI, 6 equiv **Br-PDI**, NEt_3/toluene, 80°C, 47%. (b) Optimized geometries of **Py-e-PDI**, left: side view; right: top view, as calculated from density functional theory (DFT).

In order to reveal the intramolecular steric hindrance, optimized ground state geometry of **Py-e-PDI** was calculated using Gaussian 09 software package at the B3LYP/6-31G (d, p) level of theory in the gas phase using density functional theory (DFT). In the calculations, the alkyl side chains of the molecule were replaced by methyl groups. The corresponding ground-state geometries (side view and top view) were shown in **Fig. 2b**. Normally, the introduction of C-C triple bond can remarkably enlarge the space between two connected groups and thus largely reduce the steric hindrance between them. As expected, in the **Py-e-PDI** model, four PDI units lie nearly in the plane of pyrene core with interplanar angle of only 8°, which leads to less intramolecular twist. Such geometry is beneficial for improving intermolecular packing and thus enhances the charge-transporting ability of the NF acceptor.

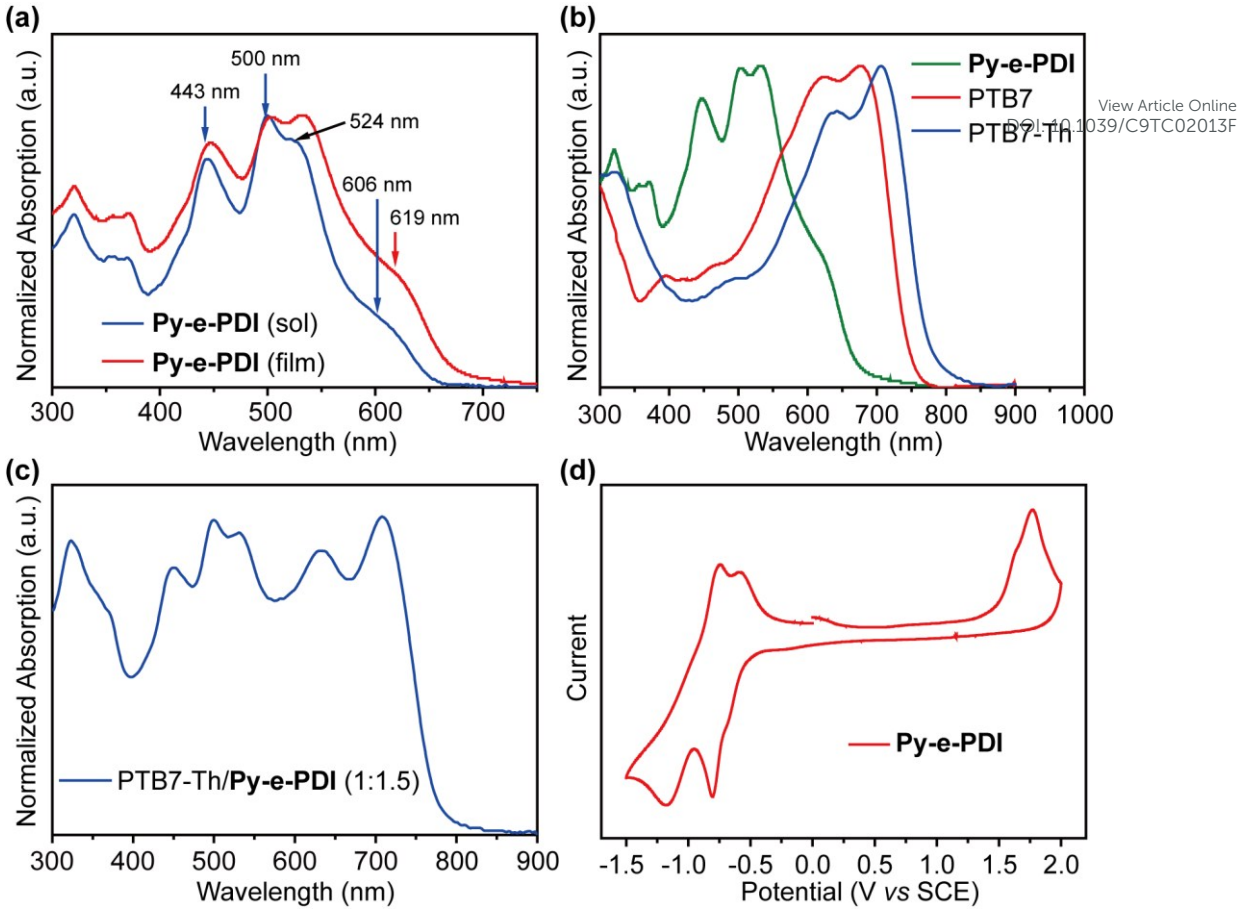

Fig. 3. UV/vis absorption spectra of (a) **Py-e-PDI** in toluene solutions and as-casted films, (b) **Py-e-PDI** film, PTB7 film and PTB7-Th films, (c) PTB7-Th/**Py-e-PDI** blend film, respectively. (d) Cyclic voltammogram of the **Py-e-PDI** thin film.

Optical Properties.

The optical properties of **Py-e-PDI** were characterized using UV−vis absorption spectroscopy. **Fig. 3a** shows the absorption spectra of this PDI derivative in dilute toluene solution and in thin film. In toluene solution, **Py-e-PDI** showed several distinct absorption bands including a weak band in the shorter wavelength region and a strong band in the longer wavelength region (450–650 nm). Noticeably, an obvious vibronic structure was observed for both absorption bands. The shorter wavelength absorption band(300–450 nm) is associated with 1,3,5,7-tetraethynylpyrene core[55], while the longer wavelength absorption originates from the intramolecular charge transfer (ICT) is associated with the PDI. Interestingly, in dilute solution, apart from the intense absorption in the region of 450-650 nm, a new small band at 606 nm occurs to **Py-e-PDI**. However, this shoulder peak still exists even if the dilute solution was heated to 70°C (**Fig. S6**). It is obvious that the longest wavelength feature is not assigned to an aggregate-based feature and probably originates from

pyrene-to-PDI charge-transfer. In thin film, the absorption band of **Py-e-PDI** is significantly broadened at the long-wavelength direction close to the absorption edge and extends the absorption onset to 675 nm, yielding an optical band gap of 1.83 eV. Additionally, the small absorption band at around 600 nm was clearly red-shifted (13 nm) and became more evident. But mostly importantly, to evaluate the new acceptor and maximize the cell efficiency, the donor polymers with complementary absorption must be found. **Fig. 3b** shows that the absorptions of both PTB7 and PTB7-Th donor polymers are complementary to that of **Py-e-PDI**. Nevertheless, since the absorption of PTB7-Th mainly lies in the range of 550–800 nm, the PTB7-Th/**Py-e-PDI** blends (**Fig. 3c**) could produce extended absorption spectra to favors solar energy harvesting.

Electrochemical Properties.

Cyclic voltammetry measurement was performed to determine the HOMO and LUMO of the novel PDI derivative. As shown in **Fig. 3d**, **Py-e-PDI** undergoes a reversible multiple-electron reduction originating from successive reduction of the peripheral PDI units. The onset reduction potential and onset oxidation potential are found to be -0.54 and 1.50 V (versus a saturated calomel electrode (SCE)). Therefore, the LUMO and HOMO energy levels are calculated to be -3.86 eV and -5.90 eV, respectively. It is worth noting that, based a comparison, the HOMO and LUMO offsets between PTB7-Th and **Py-e-PDI** is 0.68 eV and 0.20 eV, respectively. Although the LUMO offset is less than 0.3 eV, more and more studies revealed that an energy offset below 0.3 eV was also sufficient for charge separation in fullerene-free solar cells [56].

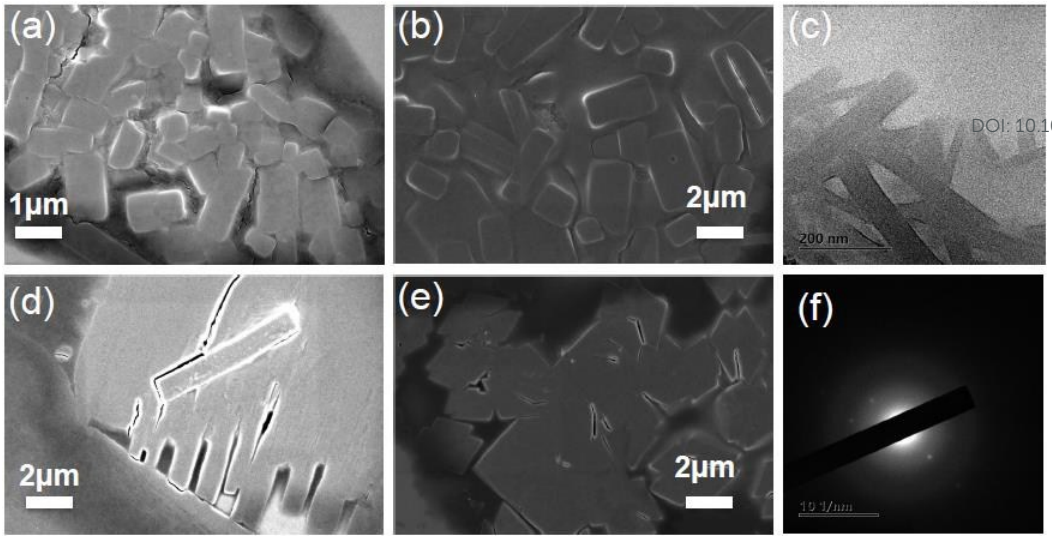

View Article Online
DOI: 10.1039/C9TC02013F

Fig. 4. SEM images of pure **Py-e-PDI** film drop-casted from toluene solution (a, b) and chlorobenzene solution (d, e). (a, d) as-casted and (b, e) thermal annealing at 100°C for 1 h, respectively. (c)TEM image and (f)electron diffraction of thermal annealing sample from chlorobenzene solution.

Morphology of the Self-Assembled Nanostructures.

Now that solution-processed manufacturing technology is employed to fabricate the organic semiconductor materials into thin-film active layer in organic optoelectronic devices, in all probability, the intrinsic molecular self-assemblies of the organic materials are involved. The morphology of self-assembled nanostructure of **Py-e-PDI** was investigated using scanning electron microscopy(SEM) and transmission electron microscope(TEM). As shown in **Fig. 4**, interestingly, planar **Py-e-PDI** assembled into highly ordered structure. A close examination of the structures deposited from dilute toluene and chlorobenzene solution revealed that some rectangular flakes with different size (from hundreds of nanometer to several micron) parallel to substrate were formed (**Fig. 4a** and **4b**). Moreover, for the sample prepared from chlorobenzene solution, thermal annealing results in a slight increasement of order in the morphologies(**Fig. 4e**). Additional experiments with TEM confirmed the existence of micron flakes (**Fig. 4c**). Furthermore, electron diffraction has been used to determine the molecular packing structure of self-assembled small molecule. As shown in **Fig. 4f**, data quickly collected for **Py-e-PDI** showed patterns consistent with highly crystalline structures but are not sufficient for further analysis. In particular, it can be expected that a **Py-e-PDI** film with highly ordered morphologies will exhibit better charge transporting properties.[57]

View Article Online
DOI: 10.1039/C9TC02013F

Table 1. Photovoltaic parameters of the OSCs based on PTB7-Th/**Py-e-PDI** blends.

D/A ratio	Solvent additive	V_{oc}/V	J_{sc}/mAcm^{-2}	FF/%	PCE/%[a]
1:1.5	none	0.80	15.8	49.8	5.89±0.21(6.10)
1:1.5	0.5%DIO	0.80	17.2	56.2	7.41±0.18(7.59)
1:1.5	1.0%DIO	0.78	13.3	50.6	5.12±0.20(5.32)
1:1.5	1.5%DIO	0.77	7.78	45.1	2.64±0.08(2.72)

[a]Average value from seven devices.

Photovoltaic performance

Py-e-PDI was used in bulk heterojunction solar cells, pairing PTB7-Th as the donor material due to their complementary absorptions and appropriately matched energy levels. OSCs were fabricated with the inverted configuration of ITO/ZnO/PTB7-Th:**Py-e-PDI** /MoO3/Ag and tested under simulated 100 mW cm^{-2} AM 1.5G illumination. First, we performed the optimization of photovoltaic performance of the OSCs of PTB7-Th: **Py-e-PDI** blends by changing the D/A weight ratios from 1.5:1 to 1:1.5. The details on the effects of the blend ratios, the thermal annealing and the thickness of active layers are provided in **Table S1**. The solar cells with 1:1.5 blend ratio show optimized power conversion efficiency (*PCE*) of 6.10% with J_{sc} of 15.8 mA cm^{-2}, V_{oc} of 0.90 V, and FF of 49.8%. Similar to most of reported PTB7-Th involved OSCs, thermal annealing has no positive effect in improving device performance based on the **Py-e-PDI** acceptor. Nevertheless, 1,8-diiodooctane (DIO) as solvent additive was proved effective to further enhance the performance of devices. As shown in **Table 1**, addition of a small amount of DIO (0.5% v/v) substantially improved the PCE from 6.10% to 7.59%, which is the highest PCE. It is worth noting that the PCE enhancement comes from the obvious increase of both *FF* and J_{sc} despite reduced V_{oc}. However, a deterioration of the performance is observed when continuing to increase the concentration of DIO. The current density−voltage (*J*−*V*) characteristics of the optimized device are presented in **Fig. 5a**.

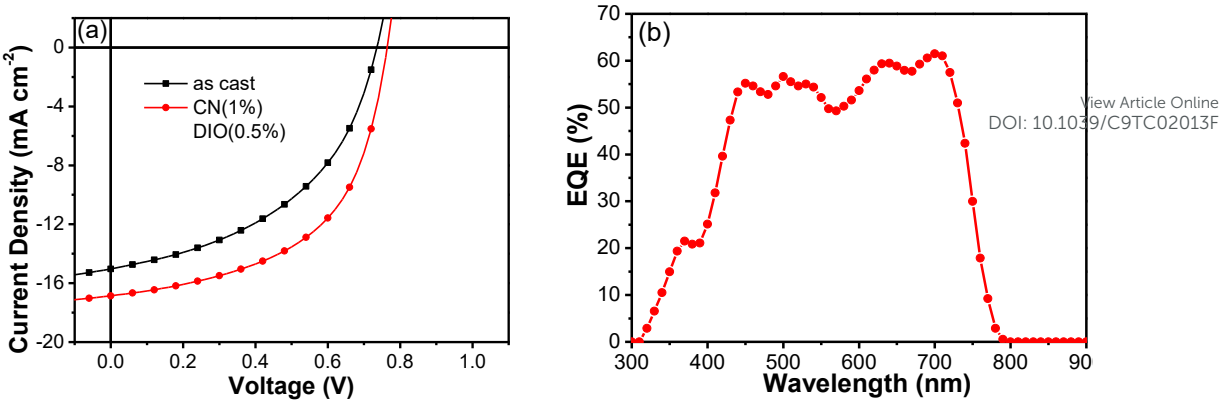

View Article Online
DOI: 10.1039/C9TC02013F

Fig. 5. (a) *J*−*V* characteristics of PTB7-Th/**Py-e-PDI** based OSCs without/with 0.5% DIO as solvent additive. (b) EQE of PTB7-Th/**Py-e-PDI** based OSCs with 0.5% DIO.

The external quantum efficiency (*EQE*) plot of optimized solar cell device based on **Py-e-PDI** is shown in **Fig. 5b**. The *EQE* curve covers a broad spectral response from 300 to 800 nm. Apparently, the range of 330–580 nm is dominantly from the photocurrent contributed by NF acceptor. One can found that obvious difference exists in the range of 300-400nm when comparing the *EQE* curve with the absorption of PTB7-Th/**Py-e-PDI** blend film (**Fig. 3c**), indicating a less efficient incident photon-to-current conversion efficiency in this range.

Space-charge-limited current (SCLC) mobilities of the pristine acceptor and blend films were measured. The structure of the hole-only devices is ITO/PEDOT:PSS/active layer/MoO3/Al, and the structure of the electron-only devices is ITO/PFN/active layer/PFN/Al. The pure **Py-e-PDI** film exhibited relatively high electron mobility (μ_e) of $(3.77 \pm 0.8) \times 10^{-4}$ cm^2 V^{-1} s^{-1}, suggesting ordered molecular packing in pristine films. However, normally, when blending with donor polymers, the electron mobility decreased largely due to reduced ordered structure. The PTB7-Th:**Py-e-PDI** blend with 0.5%DIO showed a hole mobility(μ_h) of $(1.70 \pm 0.4) \times 10^{-4}$ cm^2 V^{-1} s^{-1} and an electron mobility of $(5.97 \pm 0.7) \times 10^{-5}$ cm^2 V^{-1} s^{-1}. Clearly, quite balanced hole and electron mobilities ($\mu_h/\mu_e = 2.8 \pm 0.3$) is observed for this optimized blend. SCLC *J*-*V* plots is provided in **Fig. S7**.

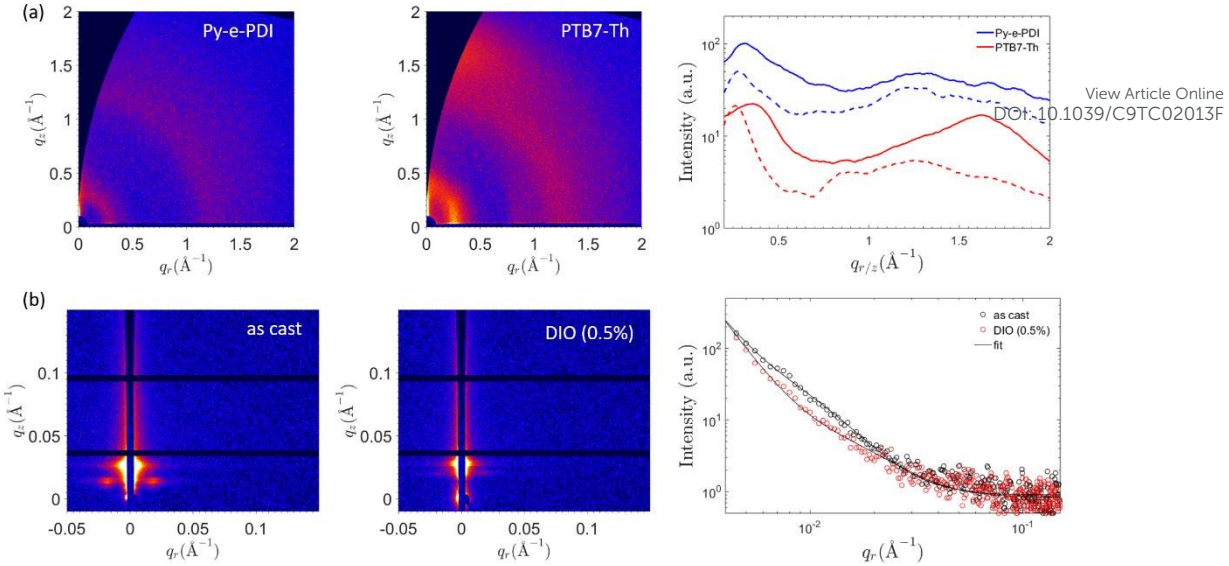

Fig. 6. (a) 2D GIWAXS scattering patterns of as-cast pure **Py-e-PDI** and PTB7-Th films and the corresponding scattering profiles in the in-plane (dashes lines) and out-of-plane (solid lines) directions. (b) 2D GISAXS scattering patterns of PTB7-Th/**Py-e-PDI** blends films as cast (left) and with 0.5% DIO (right) and the corresponding scattering profiles in the in-plane direction.

Grazing-incidence wide-angle X-ray scattering (GIWAXS) measurements were carried out to reveal the morphology structure of as-cast pure **Py-e-PDI** and PTB7-Th films[58]. As shown in **Fig. 6(a)**, the lamellar distance of **Py-e-PDI** is 22.0 Å (q ~ 0.285 $Å^{-1}$), while the face to face stacking distance is 4.91 Å (q ~ 1.28 $Å^{-1}$) with a random orientation. PTB7-Th has a face-on orientation with lamellar distance of 24.2 Å (q ~ 0.260 $Å^{-1}$) and a π-π stacking distance of 3.88 Å (q ~ 1.62 $Å^{-1}$). Grazing-incidence small-angle X-ray scattering (GISAXS) measurements were employed to investigate the nanoscale phase separation information of these blend thin films[59]. The two-dimensional GISAXS patterns and the corresponding in-plane intensity profiles were presented in **Fig. 6(b)**. We adopted a fractal-like network model to account for the scattering contribution from the acceptor domains. The uplift in the small q (<0.006 $Å^{-1}$) regions were fitted with q^{-4} dependence to account for scattering resulted either from the surface roughness of the film or from the tail of a large amorphous regime[60]. The acceptor domain sizes (2Rg) of as-cast PTB7-Th/**Py-e-PDI** film are estimated to be 42.2 nm. When 0.5% DIO was added, the domain size decreased substantially to 20.5 nm. The smaller pure phase domain size would benefit to the charge separation thus increase the J_{sc} and *FF*. The results are consistent with the device performance.

Conclusion.

In this study, we introduced pyrene unit as core to generate moderately planar PDI-tetramer based NF acceptors. DFT calculations revealed that the nonfused **Py-e-PDI** displayed reduced intramolecular twisting owing to acetylene linker and thus showed obvious crystallinity. GISAXS characterization showed that the acceptor domain sizes (2Rg) of as-cast PTB7-Th/**Py-e-PDI** film were estimated to be 42.2 nm. When 0.5% DIO was added, the domain size decreased substantially to 20.5 nm. The smaller pure phase domain size contributed to the effective charge separation thus increased the J_{sc} and *FF*. The optimized solar cells based on PTB7-Th/**Py-e-PDI** (1:1.5, 0.5%DIO) have resulted in PCE up to 7.59%, which is among highest reported efficiencies for nonfused PDI based acceptors. Most importantly, this result demonstrates that using PAH as core combined with acetylene spacer to construct multiple PDI derivatives is an effective strategy for designing high performance non-fullerene OSC acceptors.

Experimental

Materials.

All reagents were obtained from commercial suppliers and used as received. Toluene was dried over sodium/ benzophenone and freshly distilled prior to use. Triethylamine was dried over solid KOH.

Measurements and Instruments.

NMR spectra were recorded on a Bruker DPX 400 (^{1}H NMR 400, 500 MHz) spectrometer. The mass spectra were obtained using an Ion-Spec 4.7 T HiRes MALDI instrument. UV absorption spectra were obtained using a Scinco S-3150 UV/vis spectrophotometer. TGA measurements were performed on a Netzsch TG209 apparatus. The electrochemical cyclic voltammogram was obtained using a CHI 660C electrochemical workstation with Pt disk, Pt plate, and standard calomel electrode (SCE) as working electrode, counter electrode, and reference electrode, respectively, in a 0.1 mol/L tetrabutylammonium hexafluorophosphate (Bu_4NPF_6) CH_2Cl_2 solution or CH_3CN solution. The

surface morphologies of pure **Py-e-PDI** films were examined by scanning electron microscopy (Zeiss ultra plus and HITACHI S-4800) with an energy dispersive X-ray spectroscopy detector. TEM was performed with a JEOL JEM-2100 microscope operating at 200 kV. The selected-area electron diffraction (SAED) pattern was collected using the same instrument. Samples for TEM were prepared by dropping on the amorphous carbon film supported on a copper grid.

DFT calculation. Geometry optimizations were carried out by the density functional theory (DFT) method at the B3LYP/6-31G level. All the calculations were performed using Gaussian 09 program.

Device Fabrication and Characterization.

Organic solar cells were fabricated on glass substrates commercially pre-coated with a layer of indium tin oxide (ITO) with the inverted structure of ITO/ZnO/PTB7-Th:**Py-e-PDI**/MoO3/Ag. Prior to fabrication, the substrates were cleaned using detergent, deionized water, acetone and isopropanol consecutively every 15 min and then treated in an ultraviolet ozone generator for 15 min. A thin layer of sol–gel ZnO (≈ 40 nm) was spin coated onto precleaned ITO-coated glass substrates and then annealed at 180 ^{o}C for 15 min. The PTB7-Th/**Py-e-PDI** active layers were deposited from 20 mg mL^{-1} solutions without or with DIO as the additive in chlorobenzene by spin-coating at 3000 rpm, resulting in an active layer thickness of about 100 nm. MoO_3 (10 nm) and Ag (100 nm) were evaporated through a shadow mask, giving an active area of 5.2 mm^2 per device.

The current–voltage (*J*–*V*) curves were measured with Keithley 2400 measurement source units at room temperature in air. The photocurrent was measured under a calibrated solar simulator (Abet 300 W) at 100 mW cm^{-2}, and the light intensity was calibrated with a standard silicon photovoltaic reference cell. External quantum efficiency (EQE) spectrum was measured with Stanford lock-in amplifier 8300 unit.

The hole and electron mobilities of **Py-e-PDI** and blends were measured using the space-charge-limited current (SCLC) method. Hole-only devices were fabricated in a structure of

ITO/PEDOT:PSS/pure **Py-e-PDI** or PTB7-Th/**Py-e-PDI**/MoO_3(10 nm)/Al (100 nm). Electron-only devices were fabricated in a structure of ITO/PFN/ PTB7-Th:**Py-e-PDI** /PFN/Al. The device characteristics were extracted by modeling the dark current under forward bias using the SCLC expression described by the Mott-Gurney law.

Morphology Characterization.

GIWAXS and GISAXS measurements were carried out with a Xeuss 2.0 SAXS/WAXS laboratory beamline using a Cu X-ray source (8.05 keV, 1.54 Å) and a Pilatus3R 300K detector. The incidence angle is 0.2º.

Synthetic procedures.

Compound **2**. 1,3,6,8-Tetrabromopyrene (0.25 g, 0.48 mmol), bis(triphenylphosphine)palladium(II) dichloride (68 mg, 0.10 mmol), copper(I) iodide (36 mg, 0.19 mmol) and triphenylphosphine (50 mg, 0.19 mmol) were placed in a two-neck round-bottom flask under argon, and then anhydrous triethylamine (10 mL) and toluene (3 mL) were added via a syringe. While stirring, the reaction mixture was heated to 60 ◦C and trimethylsilylethyne (0.28 g, 2.88 mmol) injected. The resulted mixture was brought to reflux overnight and then cooled down to room temperature. The reaction was quenched with water, and the layers were separated. The aqueous phase was extracted with CH_2Cl_2 three times, the combined organic phase was washed with brine, and then dried over anhydrous Na_2SO_4. After removal of the solvent under reduced pressure, the crude product was purified by column chromatography (silica gel, hexane) to afford compound **2** an orange solid 228mg (yield: 81%). ^{1}H NMR(400 MHz, $CDCl_3$) δ 8.61 (m, 4 H), 8.32 (s, 2H), 0.38 (s, 36 H).

Compound **3**. Compound **2** (1 g, 1.7 mmol) was suspended in methanol (100 mL). K_2CO_3 (1.9 g, 13.6 mmol) was added and the reaction mixture stirred overnight and then poured into water (500 mL) and filtered. The filter was washed with water until the filtrate was neutral to afford compound **3** as a slightly brown solid 51mg. compound **3** is insoluble in common solvents and was used next

reaction without NMR characterization.

Py-e-PDI. To a 50 mL two necked round-bottom flask were added compound **3** (29.8 mg, 0.1 mmol), **PDI-Br**(416mg, 0.5 mmol), anhydrous toluene (12 mL) and triethylamine (6 mL), and then the mixture was deoxygenated with argon for 30 min before $Pd(PPh_3)_4$ (11.55 mg, 0.01mmol) and CuI (1.9 mg, 0.01mmol) were added. The resulted mixture was stirred at 80 °C for 72 h under argon. After cooled to room temperature, the reaction was quenched with water, and the layers were separated. The aqueous phase was extracted with CH_2Cl_2 three times, the combined organic phase was washed with brine, and then dried over anhydrous Na_2SO_4. After removal of the solvent under reduced pressure, the crude product was purified by column chromatography (silica gel, CH_2Cl_2/hexane) to afford **Py-e-PDI** as a purple solid 155mg (yield: 48%). ^{1}H NMR (400 MHz, 1, 2-dichlorobenzene-d_4) δ 10.41-11.26 (m, 4 H), 9.14-9.82 (m, 10H), 8.61-9.09 (m, 8H), 8.09-8.50 (m, 12H), 5.43-5.73 (s, 4H),4.87-5.33 (m, 4H),0.55-2.77(m, 208H). MALDI-TOF-MS: m/z calculated for $C_{224}H_{250}N_8O_{16}$: 3307.89 m/z found 3307.59. HRMS(MALD): Calcd for $C_{224}H_{250}N_8O_{16}$: 3307.8995; Found: 3307.8960; Anal. Calcd for $C_{224}H_{250}N_8O_{16}$: C, 81.27; H, 7.61; N, 3.38. Found: C, 80.76; H, 8.01;N, 3.36. Raman spectra: 2192 cm^{-1} (C≡C).

Supporting Information. ^{1}HNMR spectra, Raman spectra, TGA curves, contact angle, SCLC *J-V* plots, 2D GIWAXS scattering patterns and additional photovoltaic parameters.

***Corresponding Author**

wan_junhua@hznu.edu.cn, quzr@hznu.edu.cn, hzchen@zju.edu.cn

Author Contributions

[#] These authors contributed equally

Conflicts of interest.

There are no conflicts to declare

View Article Online
DOI: 10.1039/C9TC02013F

Acknowledgment

This work was supported by the National Natural Science Foundation of China (No. 21372057) and by Zhejiang Provincial Natural Science Foundation of China (LY18B020014). X. Lu acknowledges the financial support from CUHK direct grant.

Reference.

1. J. B. Zhao, Y. K. Li, G. F. Yang, K. Jiang, H. R. Lin, H. Ade, W. Ma, H. Yan. *Nat Energy*. **2016**, 1, 15027.

2. J. B. You, L. T. Dou, K. Yoshimura, T. Kato, K. Ohya, T. Moriarty, K. Emery, C. C. Chen, J. Gao, G. Li, Y. Yang. *Nat. Commun*, **2013**, 4, 1446.

3. J. Q. Zhang, Y. J. Zhang, J. Fang, K. Lu, Z. Y. Wang, W. Ma, Z. X. Wei. *J. Am. Chem. Soc.*, **2015**, *137*, 8176–8183.

4. S. P. Zhang, L. Ye, W. C. Zhao, B. Yang, Q. Wang, J. H. Hou. *Sci. China Chem.*, **2015**, 58, 248-256.

5. C. B. Nielsen, S. Holliday, H. Y. Chen, S. J. Cryer, I. McCulloch. *Acc. Chem. Res.*, **2015**, 48, 2803−2812.

6. C. L. Zhan, J. N. Yao. *Chem. Mater.*, **2016**, *28*, 1948–1964.

7. J. H. Hou, O. Inganas, R. H. Friend, F. Gao, *Nat. Mater.*, **2018**, 17, 119-128.

8. C. Yan, S. Barlow, Z. Wang, H. Yan, A. K-Y. Jen, S. R. Marder, X. W. Zhan, *Nat. Rev. Mater.*, **2018**, 3, 18003.

9. S. Li, L. Zhan, F. Liu, J. Ren, M. Shi, C-Z. Li, T. P. Russell, H. Chen, *Adv. Mater.* **2018**, *30*, 1705208.

10. S. Zhang, Y. Qin, J. Zhu, J. Hou, *Adv. Mater.*, **2018**, 30, 1800868.

11. S. Li, L. Ye, W. Zhao, H. Yan, B. Yang, D. Liu, W. Li, H. Ade, J. Hou, *J. Am. Chem. Soc.*, **2018**, 23, 7159–7163.

12. J. Yuan, Y. Zhang, L. Zhou, G. Zhang, H-L. Yip, T-K. Lau, X. Lu, C. Zhu, H. Peng, P. A. Johnson, M. Leclerc, Y. Cao, J. Ulanski, Y. Li, Y. Zou. *Joule*, **2019**, 3, 1140-1151.

View Article Online
DOI: 10.1039/C9TC02013F

13. L. Meng, Y. Zhang, X. Wan, C. Li, X. Zhang, Y. Wang, X. Ke, Z. Xiao, L. Ding, R. Xia, H-Y. Yip, Y. Cao, Y. Chen. *Science*, **2018**,361, 1094-1098.

14. J. J. Feng, W. Jiang, Z. H. Wang. *Chem. Asian J*. **2018**, *13*, 20–30.

15.G. Y. Zhang, J. B. Zhao, P. C. Y. Chow, K. Jiang, J. Q. Zhang, Z. L. Zhu, J. Zhang, F. Huang, H. Yan. *Chem. Rev*., **2018**, 118, 3447–3507.

16. Z. T. Liu, Y. Wu, Q. Zhang, X. Gao. *J. Mater. Chem. A*, 2016, **4**, 17604-17622.

17. F. Fernandez-Lazaro, N. Zink-Lorre, A. Sastre-Santos. *J. Mater. Chem. A*, **2016**, 4, 9336–9346.

18. S. Rajaram, R. Shivanna, S. K. Kandappa, K. S. Narayan. *J. Phys. Chem. Lett.*, **2012**, *3*, 2405–2408.

19. A. Sharenko, C. M. Proctor, T. S. van der Poll, Z. B. Henson, T. Q. Nguyen, G. C. Bazan. *Adv Mater*, **2013**, 25, 4403–4406.

20. P. E. Hartnett, A. Timalsina, H. S. S. R. Matte, N. J. Zhou, X. G. Guo, W. Zhao, A. Facchetti, R. P. H. Chang, M. C. Hersam, M. R. Wasilewski, T. J. Marks. *J. Am. Chem. Soc*, **2014**, 136, 16345–16356.

21. X. Zhang, Z. H. Lu, L. Ye, C. L. Zhan, J. H. Hou, S. Q. Zhang, B. Jiang, Y. Zhao, J. H. Huang, S. L. Zhang, Y. Liu, Q. Shi, Y. Q. Liu, J. N. Yao. *Adv Mater*, **2013**, 25, 5791–5797.

22. D. Meng, D. Sun, C. M. Zhong, T. Liu, B. B. Fan, L. J. Huo, Y. Li, W. Jiang, H. Choi, T. Kim, J. Y. Kim, Y. Sun, Z. H. Wang, A. J. Heeger. *J. Am. Chem. Soc.*, **2016**, *138*, 375–380.

23. Y. Zhong, M. T. Trinh, R. S. Chen, W. Wang, P. P. Khlyabich, B. Kumar, Q. Z. Xu, C-Y. Nam, M. Y. Sfeir, C. Black, M. L. Steigerwald, Y-L. Loo, S. H. Xiao, F. Ng, X. Y. Zhu, C. Nuckolls. *J. Am. Chem. Soc.*, **2014**, *136*, 15215–15221.

24. Q. F. Yan, Y. Zhou, Y. Q. Zheng, D. H. Zhao. *Chem. Sci*, ***2013***, *4, 4389–4394.*

25. S. M. McAfee, S. V. Dayneko, P. Josse, P. Blanchard, C. Cabanetos, G. C. Welch. *Chem. Mater.*, **2017**, *29*, 1309–1314.

View Article Online
DOI: 10.1039/C9TC02013F

26. S. X. Li, W. Q. Liu, C. Z. Li, F. Liu, Y. Z. Zhang, M. M. Shi, H. Chen, T. P. Russell. *J. Mater. Chem. A*, **2016**, 4, 10659–10665.

27. Y. W. Duan, X. P. Xu, H. Yan, W. L. Wu, Z. J. Li, Q. Peng. *Adv. Mater.*, **2017**, 29, 1605115.

28. N. Liang, K. Sun, Z. Zheng, H. Yao, G. Gao, X. Meng, Z. Wang, W. Ma, J. Hou, *Adv. Energy Mater.*, **2016**, 6, 1600060.

29. Y. Lin, Y. Wang, J. Wang, J. Hou, Y. Li, D. Zhu, X. Zhan, *Adv. Mater.*, **2014**, 26, 5137−5142.

30. Y. Liu, C. Mu, K. Jiang, J. Zhao, Y. Li, L. Zhang, Z. Li, J. Y. L. Lai, H. Hu, T. Ma, R. Hu, D. Yu, X. Huang, B. Z. Tang, H. Yan, *Adv. Mater.*, **2015**, 27, 1015–1020.

31. S-Y. Liu, C-H. Wu, C-Z. Li, S-Q. Liu, K-H. Wei, H. Chen, A. K. Y. Jen, *Adv. Sci.*, **2015**, 2, 1500014.

32. J. Lee, R. Singh, D. H. Sin, H. G. Kim, K. C. Song, K. Cho, *Adv. Mater.*, **2016**, 28, 69–76.

33. J. Yi, Y. Wang, Q. Luo, Y. Lin, H. Tan, H. Wang, C.-Q. Ma, *Chem. Commun.*, **2016**, 52, 1649–1652.

34. Q. H. Wu, D. L. Zhao, M. A. Schneider, W. Chen, L. P. Yu. *J. Am. Chem. Soc*. **2016**, 138, 7248−7251.

35. Z. T. Liu, L. H. Zhang, M. Shao, Y. Wu, D. Zeng, X. Cai, J. S. Duan, X. L. Zhang, X. Gao. *ACS Appl. Mater. Interfaces*, **2018**, 10, 762–768.

36. X. Liu, T. Liu, C. Duan, J. Wang, S. Pang, W. Xiong, Y. Sun, F. Huang, Y. Cao, *J. Mater. Chem. A*. **2017**, 5, 1713−1723.

37. Z. Luo, T. Liu, W. Cheng, K. Wu, D. Xie, L. Huo, Y. Sun, C. Yang. *J. Mater. Chem. C*, **2018**, 6, 1136-1142.

38. Q. H. Wu, D. L. Zhao, J. H. Yang, V. Sharapov, Z. X. Cai, L. W. Li, N. Zhang, A.

Neshchadin, W. Chen, L. P. Yu. *Chem. Mater.*, **2017**, 29, 1127–1133.

39. J. Q. Zhang, Y. K. Li, J. C. Huang, H. W. Hu, G. Y. Zhang, T. X. Ma, P. C. Y. Chow, H. Ade, D. Pan, H. Yan. *J. Am. Chem. Soc.*, **2017**, 139, 16092–16095.

40. D. Meng, H. T. Fu, C. Y. Xiao, X. Y. Meng, T. Winands, W. Ma, W. Wei, B. B. Fan, L. J. Huo, N. L. Doltsinis, Y. Li, Y. M. Sun, Z. H. Wang. *J. Am. Chem. Soc.*, **2016**, 138, 10184–10190.

41. H. Zhong, C-H. Wu, C-Z. Li, J. Carpenter, C-C. Chueh, J-Y. Chen, H. Ade, A. K. Y. Jen. *Adv. Mater.* **2016**, *28*, 951–958.

42. P. E. Hartnett,; H. S. S. R. Matte, N. D. Eastham, N.E. Jackson, Y. Wu, L. X. Chen, M. A. Ratner, R. P. H. Chang, M. C. Hersam, M. R. Wasielewski. *Chem. Sci.* **2016**, 7, 3543−3555.

43. Y. Zhong, M. T. Trinh, R. Chen, G. E. Purdum, P. P. Khlyabich, M. Sezen, S. Oh, H. Zhu, B. Fowler, B. Zhang, W. Wang, C-Y. Nam, M. Y. Sfeir, C. T. Black, M. L. Steigerwald, Y-L. Loo, F. Ng, X. Y. Zhu, C. Nuckolls, *Nat. Commun.*, **2015**, 6, 8242.

44. M. L. Wu, J. P. Yi, L. Chen, G. Y. He, F. Chen, M. Y. Sfeir, J. L. Xia. *ACS Appl. Mater. Interfaces*, **2018**, 10, 27894–27901.

45. H. Sun, X. Song, J. Xie, P. Sun, P. Y. Gu, C. M. Liu, F. Chen, Q. C. Zhang, Z. K. Chen, W. Huang, *ACS Appl. Mater. Interfaces*, **2017**, 9, 29924–29931.

46. A. D. Zhang, C. Li, F. Yang, J. Q. Zhang, Z. H. Wang, Z. X. Wei, W. W. Li. *Angew. Chem. Int. Ed.*, **2017**, 56, 2694 –2698.

47. H. R. Lin, S. S. Chen, H. W. Hu, L. Zhang, T. X. Ma, J. Y. L. Lai, Z. K. Li, A. J. Qin, X. H. Huang, B. Z. Tang, H. Yan. *Adv. Mater.* **2016**, 28, 8546–8551.

48. H. Wang, L. Chen,Y. Xiao. *J. Mater. Chem. A*, **2017**, 5, 22288–22296.

49. H. Wang, L. Cheng, Y. Xiao. *J. Mater. Chem. C*, **2019**, 7, 835-842.

50. W. Chen, X. Yang, G. Long, X. Wan, Y. Chen, Q. Zhang. *J. Mater. Chem. C*, **2015**, 3, 4698-4705.

51. G. Li, Y. Zhang, T. Liu, S. Wang, D. Li, J. Li, F. Li, L-M. Yang, Z. Luo, C. Yang, H. Yan, P.

Hao, Q. Shang, B. Tang. *J. Mater. Chem. C*, **2018**, 6, 11111-11117.

52. H. Wang, M. Li, Y. Liu, J. Song, C. Li, Z. Bo. *J. Mater. Chem. C*, **2019**, 7, 819-825.

53. S. Zhou, G. Feng, D. Xia, C. Li, Y. Wu, W. Li, *Acta Phys. -Chim. Sin*., **2018**, 34, 344-347.

54. Y. Guo, A. Zhang, C. Li, W. Li, D. Zhu, *Chin. Chem. Lett*. **2018**, 29, 371-373.

55. H. Lu, Q. Wang, Z. Li, G. Lai, J. Jiang, Z. Shen. *Org. Biomol. Chem.*, **2011**, 9, 4558–4562.

56. J. Liu, S. S. Chen, D. P. Qian, B. Gautam, G. F. Yang, J. B. Zhao, J. Bergqvist, F. L. Zhang, W. Ma, H. Ade, O. Inganäs, K. Gundogdu, F. Gao, H. Yan. *Nature Energy* **2016**, 1, 16089.

57. Z. Hu, R. Xu, S. Dong, K. Lin, J. Liu, F. Huang, Y. Cao. *Mater. Horiz.*, **2017**, 4, 88-97.

58. J. Mai, Y. Xiao, G. Zhou, J. Wang, J. Zhu, N. Zhao, X. Zhan, X. Lu. *Advanced Materials*, **2018**, 1802888.

59. J. Mai, T-K. Lau, J. Li, S-H. Peng, C-S. Hsu, U-S. Jeng, J. Zeng, N. Zhao, X. Xiao, X. Lu. *Chem. Mater*., **2016**, 28, 6186-6195.

60. H. Shen, W. Zhang, M. E. Mackay, *J. Polym. Sci. Pol. Phys*., **2014**, 52**,** 387-396.

View Article Online
DOI: 10.1039/C9TC02013F

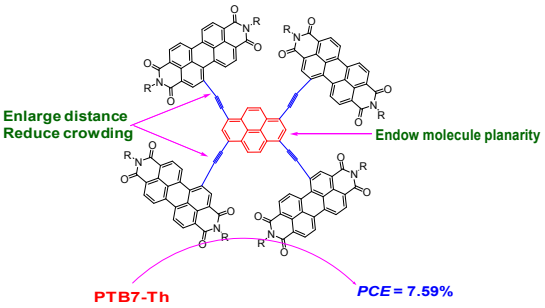

The pyrene core and significantly reduced intramolecular steric hindrance endows nonfused PDI-tetramer with moderate planarity and good self-assembly property.